Available online at www.sciencedirect.com

ScienceDirect

Ceramics International 40 (2014) 2063–2071

CERAMICS INTERNATIONAL

www.elsevier.com/locate/ceramint

# Interfacial and mechanical characterization of yttria-stabilized zirconia (YSZ) to stainless steel joints fabricated using Ag–Cu–Ti interlayers

Kun-Lin Lin[a], Mrityunjay Singh[b], Rajiv Asthana[c,*], Chao-Hsien Lin[d]

[a]National Nano Device Laboratories, Hsinchu 300, Taiwan
[b]Ohio Aerospace Institute, 22800 Cedar Point Road, Cleveland, OH 44142, USA
[c]Engineering and Technology Department, University of Wisconsin–Stout, Menomonie, WI 54751, USA
[d]Institute of Imaging and Biomedical Photonics, National Chiao Tung University, Hsinchu 300, Taiwan

Received 3 March 2013; received in revised form 24 July 2013; accepted 25 July 2013
Available online 2 August 2013

**Abstract**

An Ag–26.7Cu–4.5Ti metallic interlayer was used to join yttria-stabilized zirconia (YSZ) and stainless steel for solid oxide fuel cell (SOFC) applications. Scanning electron microscopy (SEM), transmission electron microscopy (TEM), and energy dispersive spectroscopy (EDS) were used to characterize the joint microstructure. The bond strength and hermeticity of steel/metallic interlayer/YSZ joints were also evaluated. TEM analysis revealed that the Fe from the steel reacted with Ti of the interlayer to form $Fe_2Ti$ near the steel/Ag–26.7Cu–4.5Ti interface. At the Ag–26.7Cu–4.5Ti interlayer/YSZ interface, $Ti_2O_3$ and $Fe_2Ti_4O$ reaction layers formed near the YSZ and the interlayer, respectively. While titanium reacted with oxygen from YSZ to form titanium oxide ($Ti_2O_3$), Fe diffused toward the YSZ to react with titanium oxide to form the $Fe_2Ti_4O$ layer. The tensile and shear strengths of the joints, evaluated according to "ISO 13124" test method, were $16.7 \pm 4.8$ and $40.2 \pm 8.2$ MPa, respectively. Nano-indentation hardness was characterized across the steel/Ag–26.7Cu–4.5Ti interlayer/YSZ joint. The hermeticity of the joint was measured by using He leakage tests. The leak rate of the joined assembly was $1.5 \pm 1.1 \times 10^{-9}$ mbar $\ell$/s, indicating good hermeticity of joints.


*Keywords:* Oxide materials; Liquid–solid reactions; Scanning electron microscopy; Transmission electron microscopy; Nano-indentation

## 1. Introduction

There is a high demand for robust integration technologies to join yttria-stabilized zirconia (YSZ), the most commonly used electrolyte material in solid oxide fuel cells (SOFCs), to metal frames or interconnects made from stainless steel. A number of glass and metallic sealants have been developed and tested with varying degree of success for applications in SOFCs [1–6]. Sealants in SOFC are always exposed to oxidizing atmosphere (e.g., air) on the cathode side and a wet fuel gas on the anode side. Thus, hermetic seals are extremely important under the SOFC operating conditions, as minute leaks in seals can affect the cell potential and degrade cell performance [5,6]. Metallic sealants have been shown to provide rigid sealing and better stress accommodation than ceramic sealants [1,5,6]. In order to sustain the high-temperature operation under dual atmosphere, the metallic sealants should be judiciously chosen for oxidation resistance and long-term chemical stability. A number of systems based on noble metals such as silver, gold, and platinum have shown interesting properties and they exhibit potential for wide scale applications [1,3,5]. Although the functions of different seals in the SOFC could be very different depending upon the design, the most crucial property, required of all SOFC seals, is hermeticity. A mismatch in the coefficients of thermal expansion (CTE) and elemental inter-diffusion between seals and cell and/or interconnect can affect hermeticity after extended service. It is, therefore, important to characterize the hermeticity (i.e., sealing effectiveness) following ageing.

*Corresponding author. Tel.: +1 715 232 2152; fax: +1 715 232 1330.
*E-mail address:* asthanar@uwstout.edu (R. Asthana).

0272-8842/$ - see front matter © 2013 Elsevier Ltd and Techna Group S.r.l. All rights reserved.
http://dx.doi.org/10.1016/j.ceramint.2013.07.119

The joining of zirconia to stainless steel or to itself has been studied by using a variety of metallic interlayers, such as those based on Ag [7–15], Cu [7,16,17], Pd [18], Au [19–21], Ni [22] as well as active composite braze interlayers [23]. Out of these interlayers, Ag-based interlayers, such as Ag–Cu–Ti [13] and Ag +CuO [2,6], have been applied in SOFC's devices. However, the nature of the reaction products at the interface between metallic interlayers and YSZ remains somewhat elusive [7,11,13,14,18, 19,22,24]. Various investigators [7,11,13,14,18,19,22,24] have used generic chemical formulae such as $Ti_xO_y$ or $TiO_x$ to represent the titanium oxide(s) at the interface between metallic interlayers and ceramics on the basis of scanning electron microscopy (SEM) and energy dispersive spectroscopy (EDS). Some researchers [9,10,25,26] have used X-ray diffraction (XRD) to identify thin layers of titanium oxides, such as TiO [9,10,25], $Ti_2O$ [25], $Ti_3O$ [26], and $Ti_6O$ [26] at the oxide/metal interface. However, XRD patterns could not be analyzed with precision on such thin ($<1$ μm) titanium oxide layers in joined samples. Besides, XRD peaks easily overlap the peaks of steel, interlayers, and YSZ, and the accuracy in the identification of titanium oxides is greatly reduced.

The detailed microstructure and composition of the interfacial reaction products at the YSZ/steel joints has never been accurately revealed because of the limitations of the characterizing techniques such as XRD, SEM and EDS. In the present work, a transmission electron microscope (TEM) equipped with EDS was used to accurately characterize the interfacial reaction phases at steel/YSZ joints made by using thin Ag–Cu–Ti interlayers. In order to accurately identify the crystal structure of titanium oxides, a series of selected area diffraction patterns (SADPs) of TEM were taken and analyzed. In addition, tensile and shear strength, hardness, and hermeticity of stainless steel/Ag–Cu–Ti interlayer/YSZ joint were also evaluated.

## 2. Experimental procedure

A corrosion-resistant ferritic stainless steel from Allegheny Ludlum and yttria-stabilized zirconia (YSZ) substrates containing 3 mol% yttria, were used in the joining experiments. The steel nominally contained 17–19% Cr, and minor alloying constituents ($<0.1$% Mn, P, Si, Ni, and Ti). The nominal compositions (in wt%) of metallic interlayer foil, obtained from Morgan Advanced Ceramics (Hayward, CA), was Ag–26.7Cu–4.5Ti ($\sim$0.10–0.12 mm thick, $T_L$: 1173 K). The YSZ and stainless steel samples for bonding and microstructural characterization were cut to 10 mm × 10 mm × 2 mm size. For hermeticity tests, YSZ and stainless steel samples, 10 mm × 10 mm × 2 mm in size, were prepared with a 2 mm diameter hole in the center. For tensile and shear strength tests, rectangular bars of YSZ and steel, 4 mm × 4 mm × 15 mm in size, were joined orthogonally and symmetrically to produce cross-bonded joints. The joining procedure consisted of placing an Ag–26.7Cu–4.5Ti interlayer between YSZ and stainless steel under a normal load of $\sim$0.3 N. In order to remove surface contaminates, all materials were pre-cleaned in acetone using ultrasound for 10 min. The sample assembly was heated to 1188 K under a vacuum of $\sim 10^{-6}$ Torr, isothermally held at the temperature for 5 min, and slowly cooled to room temperature at a controlled rate.

The microstructure of the reaction products at the interface of steel/Ag–26.7Cu–4.5Ti interlayer/YSZ joints was characterized using a TEM (Model JEM 2010Fx, JEOL Ltd., Tokyo, Japan) equipped with an EDS (Model ISIS300, Oxford Instrument Inc., London, U.K.). The crystal structures of the reaction products were characterized by analyzing the selected area diffraction patterns (SADP) accessed by using TEM and EDS. The inorganic crystal structure database (ICSD) and the crystallographic software (Diamond version 3.0 and CaRIne Crystallography 3.1) were used for the identification of the crystal structures of the phases. The cross-sectional TEM specimens of YSZ/interlayer/steel joints were prepared by mechanical polishing and focused ion beam (FIB, FEI NovaLab 600). The quantitative composition analyses were performed based on the principle of the Cliff–Lorimer [27] standardless method. Besides, in order to accurately calculate the lattice parameters of reaction products, the image magnification in TEM was calibrated using a MAG*I*CAL reference standard sample from Norrox Scientific Ltd.

The tensile and shear strength tests on joints were performed with a universal testing machine, 536M1 from Cometech Testing Machines Co., LTD. All tests were conducted using a cross-head speed of 0.5 mm/min. According to the applicable ISO test standard [28], the test rate should be sufficiently rapid, so as to complete the test within 10–30 s, thereby obtaining the maximum possible tensile strength at fracture of the interface of the cross-bonded sample. Multiple test specimens were utilized for estimating the mean interfacial tensile strength and shear strength of joints. The hermeticity (leakage) test was performed with a helium leak detector, ASM310 from Alcatel Vacuum Technology, France.

The hardness ($H$) and elastic modulus ($E$) across the joints were characterized with a nanoindenter (Picodentor HM500, Fischer, German) using a Berkovich indenter tip. The analysis method of indentation hardness defined by ISO 14577 as proposed by Oliver and Pharr [29] was used. The approach speed of the indenter was less than 1.2 μm/s. A peak force of 4.9 mN was used for all reaction products due to their small thickness. In order to evaluate the change in hardness from the steel and Ag–26.7Cu–4.5Ti interlayer to YSZ, line indents, consisting of 27 point indents with an interval of 3$\sim$4 μm, across the brazed joint were performed. The $H$ and $E$ of the reaction products were determined from the load-displacement curves.

## 3. Results and discussion

### 3.1. SEM analysis

Fig. 1(a) is a SEM backscattered electron image (BEI) of the Ag–26.7Cu–4.5Ti interlayer before joining, showing the two main Ag-rich (white region) and Cu-rich (gray region) phases. Fig. 1(b) is a SEM BEI of a steel/Ag–26.7Cu–4.5Ti/YSZ joint following bonding at 1188 K/5 min, displaying Ag-rich (white

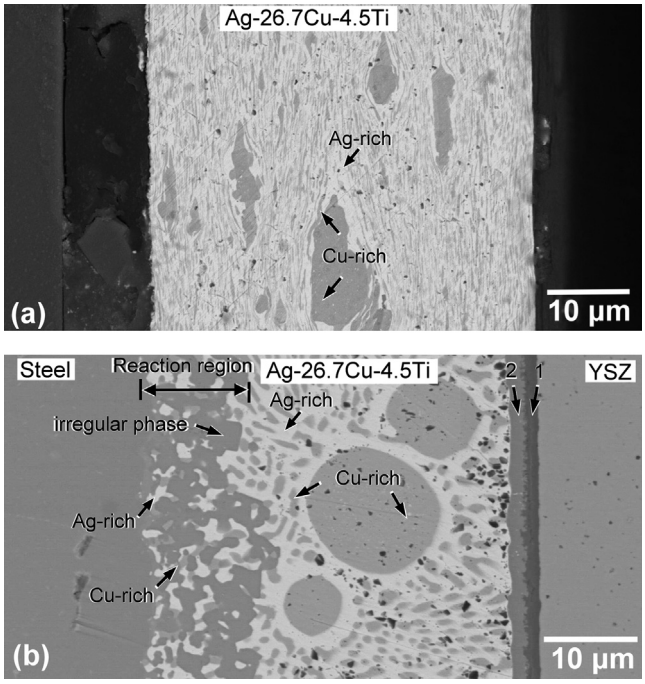


Fig. 1. Scanning electron micrograph (backscattered electron image, BEI) of the (a) Ag–26.7Cu–4.5Ti interlayer before joining, indicating Ag-rich phase (white region) and Cu-rich phase (gray region), and (b) a BEI of steel/Ag–26.7Cu–4.5Ti/YSZ interface, displaying the irregular phase (dark region) in the steel/Ag–26.7Cu–4.5Ti interface, two reaction layers (marked as "1" and "2") in the Ag–26.7Cu–4.5Ti/YSZ interface, and Ag-rich and Cu-rich phases within the interlayer.

region) and Cu-rich (gray region) phases within the Ag–26.7Cu–4.5Ti interlayer. In the steel/Ag–26.7Cu–4.5Ti interface, the reaction region consisted of Ag-rich (white) and Cu-rich (gray) regions, and an irregular phase (dark region). From the EDS of SEM, the irregular phase was identified as a Fe–Ti compound with a composition (in atom %) of 57.9 at% Fe, 32.1 at% Ti, 7.5 at% Cr, 0.8 at% Ag and 1.7 at % Cu. It is conceivable that the steel constituents, especially Fe and Cr, dissolved into the silver-based interlayers during joining to result in the formation of the irregular phase. In the Ag–26.7Cu–4.5Ti/YSZ interface, two reaction layers (marked as "1" and "2") were found at the Ag–26.7Cu–4.5Ti/YSZ interface. Similarly, from the EDS, the reaction layer "1" was identified as a Ti–O compound (40.8 at% Ti, 58.4 at% O, 0.4 at% Fe, and 0.4 at% Zr) and the reaction layer "2" was a Fe–Ti–O compound (42.5 at% Ti, 21.6 at% Fe, 27.8 at% O, 2.9 at% Cr, and 3.8 at% Cu, and 1.4 at% Zr). Transmission electron microscopy (TEM) was used to identify the phases, and determine the crystal structure and composition of the reaction products, such as Fe–Ti, Fe–Ti–O, and Ti–O compounds, and will be discussed below.

### 3.2. TEM analysis

Fig. 2(a) shows a TEM micrograph (bright-field image, BFI) of the Ag-rich and Cu-rich phases within Ag–26.7Cu–4.5Ti interlayer, corresponding with the Ag-rich and Cu-rich phases

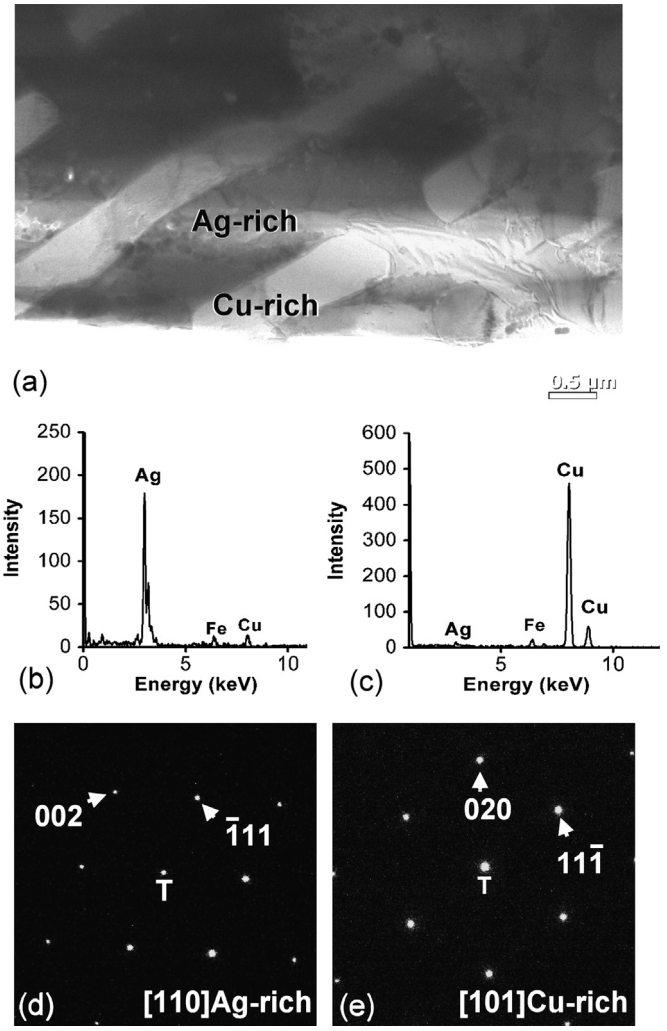


Fig. 2. (a) Transmission electron micrograph (bright-field image, BFI) of the Ag-rich and Cu-rich phases within Ag–26.7Cu–4.5Ti interlayer, corresponding with the Ag-rich and Cu-rich phases of Fig.1(b); (b, c) EDS spectra of the Ag-rich and Cu-rich phases, and (d, e) selected area diffraction patterns (SADPs) of the Ag-rich phase with zone axis of [110] and Cu-rich phase along with the zone axis of [101].

of Fig.1(b). From the EDS data shown in Fig. 2(b and c), the compositions (in atom %) of the Ag-rich and Cu-rich phases were determined to be: (87.1 Ag, 4.8 Fe, and 8.1 Cu) and (95.1 Cu, 3.2 Fe, and 1.7 Ag), respectively. Fig. 2(d and e) shows the superimposed selected area diffraction pattern (SADP) of the Ag-rich phase with zone axis of [110] and Cu-rich phase along with the zone axis of [101]. The lattice parameters of the Ag-rich and Cu-rich phases were calculated as 4.28 and 3.77 Å respectively. Obviously, the lattice parameters of Ag-rich and Cu-rich phases were a little larger than those of pure Ag and Cu (4.07 and 3.61 Å) since elemental iron from steel had dissolved in the Ag-rich or Cu-rich phases, according to the EDS data.

Fig. 3(a) shows a BFI of the steel/Ag–26.7Cu–4.5Ti interface, indicating the coexistence of the $Fe_2Ti$ phase, and the Ag-rich and Cu-rich phases corresponding with SEM images of the irregular Fe–Ti compound, and the Ag-rich and Cu-rich

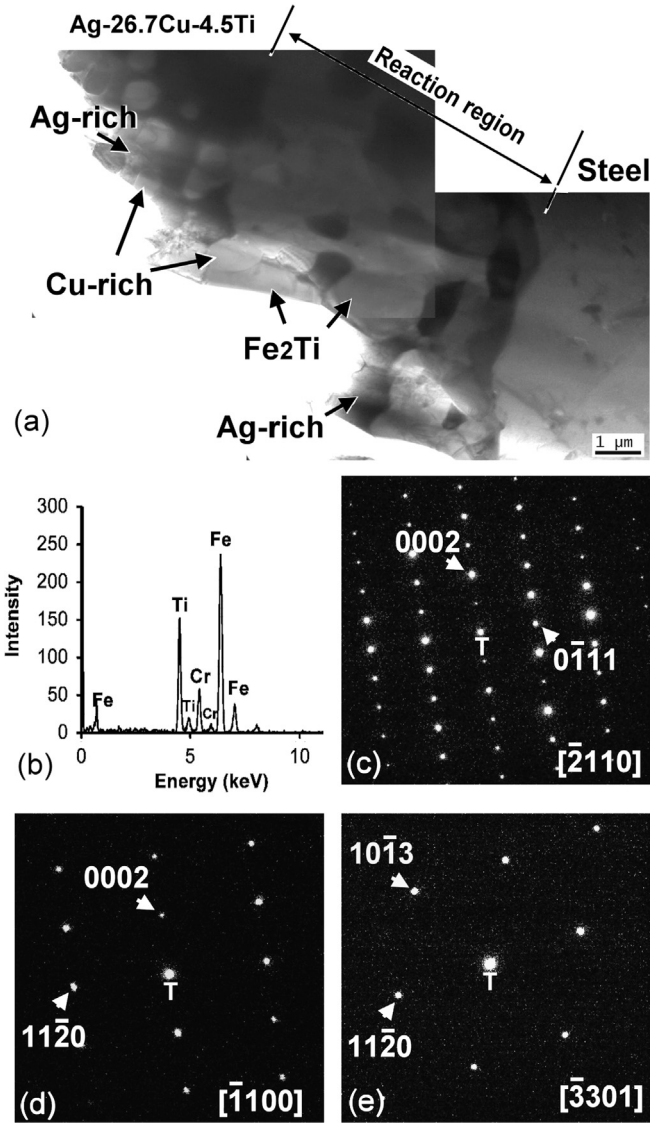


Fig. 3. (a) Transmission electron micrograph (bright-field image, BFI) of the steel/Ag–26.7Cu–4.5Ti interface, indicating the $Fe_2Ti$ phase corresponding with the irregular phase of Fig. 1(b); (b) EDS spectrum of $Fe_2Ti$ phase, and (c–e) selected area diffraction patterns (SADPs) of $Fe_2Ti$ phase with zone axes of $[\bar{2}110]$, $[\bar{1}100]$, and $[\bar{3}301]$, respectively.

phases in the reaction region of Fig. 1(b). The EDS analysis shown in Fig. 3(b) reveals that the composition of the $Fe_2Ti$ phase was 54.2 at% Fe, 31.8 at% Ti, 11.8 at% Cr, and 2.1 at% Cu. Fig. 3(c, d) shows SADPs of $Fe_2Ti$ phase with zone axes of $[\bar{2}110]$, $[\bar{1}100]$, and $[\bar{3}301]$, respectively. The lattice parameters of the $Fe_2Ti$ phase were calculated to be $a=4.97$ Å, $c=8.14$ Å and $\lambda=\beta=90^\circ$, $\gamma=120^\circ$, corresponding with the hexagonal $Fe_2Ti$ of JCPDS–ICDD # 15–0336 [$a=4.79$ Å, $c=7.80$ Å and $\lambda=\beta=90^\circ$, $\gamma=120^\circ$, space group=$P6_3/mmc$ (194)]. During the heating process, Fe from the steel diffused and reacted with the Ti of the interlayer to form the $Fe_2Ti$ phase at the steel/interlayer interface. Possible chemical reactions of Fe and Ti to form the FeTi and $Fe_2Ti$ phases and the corresponding free energy changes are [30]

$$Fe+Ti \rightarrow FeTi,\ \Delta G_{1188\ K}=-30\ kJ/mol \quad (1)$$

$$Fe+1/2Ti \rightarrow 1/2Fe_2Ti,\ \Delta G_{1188\ K}=-70\ kJ/mol \quad (2)$$

The formation of FeTi and $Fe_2Ti$ is likely because the reactions (1) and (2) have negative free energy changes; however, in the present study, only $Fe_2Ti$ was found at the steel/interlayer interface. In general, intermetallic compounds are hard and brittle, readily form cracks at the interface of joints, and degrade the joint strength. For example, in Ref. [31], $Fe_xTi_y$ intermetallic layers, about 2 μm in thickness and accompanied by cracks, had formed at the interface of steel/Ti–Cu–Ni interlayers (Ti–28Cu–12Ni, wt%). However, from the SEM (Fig. 1(b)) and TEM (Fig. 3(a)) examination in the present work, no cracks were found at the interface even though the $Fe_2Ti$ intermetallic phase had formed. This could possibly be because unlike the pure $Fe_xTi_y$ intermetallic layer that had formed at the steel/Ti–Cu–Ni interlayer joint in Ref. [31], the $Fe_2Ti$ phase in the present study was dispersed in the Ag-rich and Cu-rich regions and formed a complex reaction layer at the steel/Ag–26.7Cu–4.5Ti interface (Fig. 1(b)). Obviously, the effect of $Fe_xTi_y$ intermetallics to form either a concentrated single layer or a distributed complex reaction layer depends upon the Ti content in the metallic interlayers. If the metallic interlayers with a high Ti content react with the steel, a hard and brittle $Fe_xTi_y$ intermetallic layer would form at the interface accompanied with crack formation [31], caused by the CTE mismatch between the steel and metallic interlayers. But, if the steel was joined with the Ti-impoverished metallic interlayers, such as the Ag–26.7Cu–4.5Ti interlayers of the present study, then the reaction layer at the interface would be complex and composed of $Fe_2Ti$, Ag-rich, and Cu-rich phases rather than just pure $Fe_xTi_y$. It is believed that a composite reaction layer could be more compliant and less hard and brittle compared to a pure $Fe_xTi_y$ intermetallic layer because the plastically deformable Ag-rich and Cu-rich phases could accommodate stress to prevent crack formation at the interface. The distributive arrangement of chemical phases and stress accommodation capability of a composite layer can be captured via nano-indentation hardness profiles, and will be discussed later.

Fig. 4(a) shows the BFI of the $Ti_2O_3$ and $Fe_2Ti_4O$ phases in the Ag–26.7Cu–4.5Ti/YSZ interface, corresponding with the reaction layer "1" and "2" of Fig. 1(b). The EDS spectra of Fig. 4(b) shows the composition of $Ti_2O_3$ to be 40.5 at% Ti, 55.2 at% O, and 4.3 at% Zr, indicating minor Zr diffusion from YSZ. As for the $Fe_2Ti_4O$ phase, it is composed of 41.6 at% Ti, 27.9 at% Fe, 16.9 at% O, 7.47 at% Cr, and 3.5 at% Cu, and 2.7 at% Zr. Fig. 4(d) shows the SADPs of $Ti_2O_3$ phase with zone axes of $[0\bar{1}0]$ and $[\bar{1}\bar{2}0]$. The lattice parameters of rhombohedral $Ti_2O_3$ were calculated to be $a=b=5.26$Å, $c=14.09$ Å, $\alpha=\beta=90^\circ$, and $\gamma=120$ corresponding with the values of $Ti_2O_3$ of ICSD #9658 (crystal system: rhombohedral, space group: R-3c, space group number: 167, $a=b=5.1257$ Å, $c=13.9140$Å, $\alpha=\beta=90^\circ$, and $\gamma=120^\circ$). Until now, even though the various titanium oxides, such as TiO [9,10,25], $Ti_2O$ [25], $Ti_3O$ [26], and $Ti_6O$ [26] at

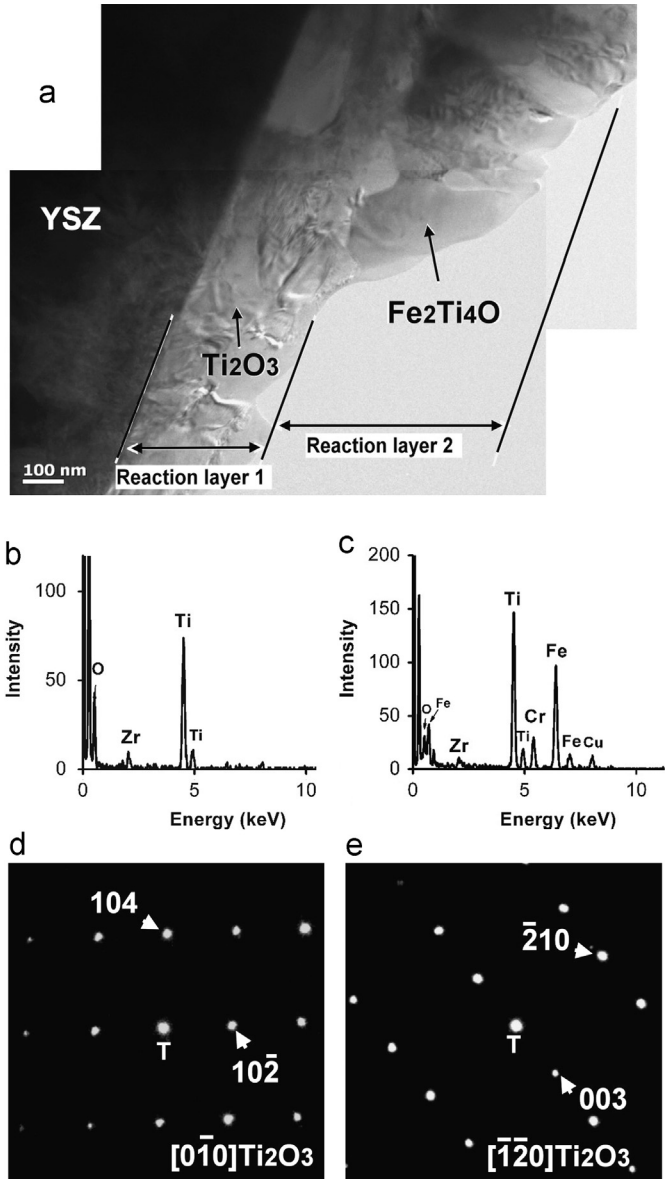


Fig. 4. (a) Transmission electron micrograph (bright-field image, BFI) of the $Ti_2O_3$ and $Fe_2Ti_4O$ phases in the Ag–26.7Cu–4.5Ti/YSZ interface, corresponding with the reaction layer "1" and "2" of Fig. 1(b), (b, c) EDS spectra of the $Ti_2O_3$ and $Fe_2Ti_4O$ phases, and (d, e) selected area diffraction patterns (SADPs) of $Ti_2O_3$ phase with zone axes of [0$\bar{1}$0] and [$\bar{1}\bar{2}$0].

the oxide/metal interface with different metallic interlayers were detected using XRD, most researchers [11,14,18,19,22,24] preferred to use generic chemical formulae $Ti_xO_y$ or $TiO_x$ to represent the titanium oxide layers at the interface based on their EDS results because of the limited resolution and the difficulty of conducting XRD on thin titanium oxide layers ($<1$ μm thick). Recently, Lin et al. [32] accurately identified the $Ti_2O_3$ phase at a 96.4Au–3Ni–0.6Ti interlayer/YSZ interface, by employing SADPs in TEM and the SADP simulations. Similarly, in the present study, $Ti_2O_3$ formation at the Ag–26.7Cu–4.5Ti/YSZ interface was proved by the EDS (Fig. 4(b)) and SADPs (Fig. 4(d, e)). Besides, Lin et al. [32] also discussed the formation mechanism and thermodynamic calculation of titanium oxide at the interface and concluded that a dissolution – reduction process rather than an oxidation–reduction process dominated the reaction of Ti with $ZrO_2$.

Apart from the $Ti_2O_3$ layer that formed at the Ag–26.7Cu–4.5Ti interlayer/YSZ interface, a $Fe_2Ti_4O$ layer corresponding with the reaction layer "1" of Figs. 1(b) and 4(a) was found in the steel/Au–3Ni–0.6Ti interlayer/YSZ joint. Fig. 5(a and b) shows the simulated and experimental SADPs of $Fe_2Ti_4O$ with zone axes of [112], [111], [213], and [101], respectively. The lattice parameters of cubic $Fe_2Ti_4O$ were calculated to be $a=b=c=11.33$Å, and $\alpha=\beta=\gamma=90^\circ$, corresponding with the values of $Fe_2Ti_4O$ of ICSD #029058 (crystal system: cubic, space group: Fd3m, space group number: 227, $a=b=c=11.31$Å, and $\alpha=\beta=\gamma=90^\circ$). Most researchers [8–10] only reported finding the titanium oxides at the interface of YSZ/YSZ and steel/YSZ joints made by using Ag–Cu–Ti interlayers. The present study is the first to report the formation of a $Fe_2Ti_4O$ layer at the interface of Ag–26.7Cu–5Ti interlayer/YSZ, apart from the titanium oxide ($Ti_2O_3$), which was reported earlier. It is possible that the iron from the steel diffused across the Ag–26.7Cu–4.5Ti interlayer to react with $Ti_2O_3$ to form the $Fe_2Ti_4O$ layer. Moreover, the diffusion distance of iron or other alloying elements from steels into metallic interlayers has been evaluated according to Nernst–Brunner equation [19,32] and indicates that the concentrations of the dissolved species (Fe, Cr, and Ni from steels) could attain saturation with 100 μm thick metallic interlayers in 5 min. bonding time. The estimates confirmed rapid dissolution and large-scale compositional changes, and supported the reaction of Fe from the steel with $Ti_2O_3$ to form $Fe_2Ti_4O$ layer near the YSZ/interlayer interface far from the steel substrate as was actually observed. The possible chemical reaction can be described by the following equation:

$$Fe+Ti_2O_3 \rightarrow 1/2Fe_2Ti_4O+O \quad (3)$$

The evolution of the microstructure of the steel/Ag–26.7Cu–4.5Ti/YSZ joint during a single thermal cycle is schematically illustrated in Fig. 6. The elemental interdiffusion took place when the steel/Ag–26.7Cu–4.5Ti/YSZ joints were formed at the joining temperature. For instance, the Fe and minor alloying constituents (Mn, Si, and Ni) from the steel dissolved into Ag–26.7Cu–4.5Ti interlayer and the active metal Ti of Ag–26.7Cu–4.5Ti interlayer diffused toward the steel and YSZ on the two sides of the joint. Upon cooling, titanium of the Ag–26.7Cu–4.5Ti interlayer reacted with the oxygen of YSZ to form a reaction layer of $Ti_2O_3$ at the interlayer/YSZ interface. In addition, Fe from the steel reacted with Ti of the interlayer to produce $Fe_2Ti$ phase, which was also composed of Cu-rich and Ag-rich phases to form a complex but compliant reaction layer at the steel/interlayer interface. Moreover, the Fe extensively diffused across the interlayer to react with $Ti_2O_3$ to form a $Fe_2Ti_4O$ reaction layer at the interlayer/$Ti_2O_3$ interface. Support for the above mechanism comes from a study on $Al_2O_3/Al_2O_3$ and $Al_2O_3$/steel joined using Ag–Cu–Ti interlayers [33], where a similar mechanism was proposed for the formation of the $Cu_2Ti_4O$ phase.

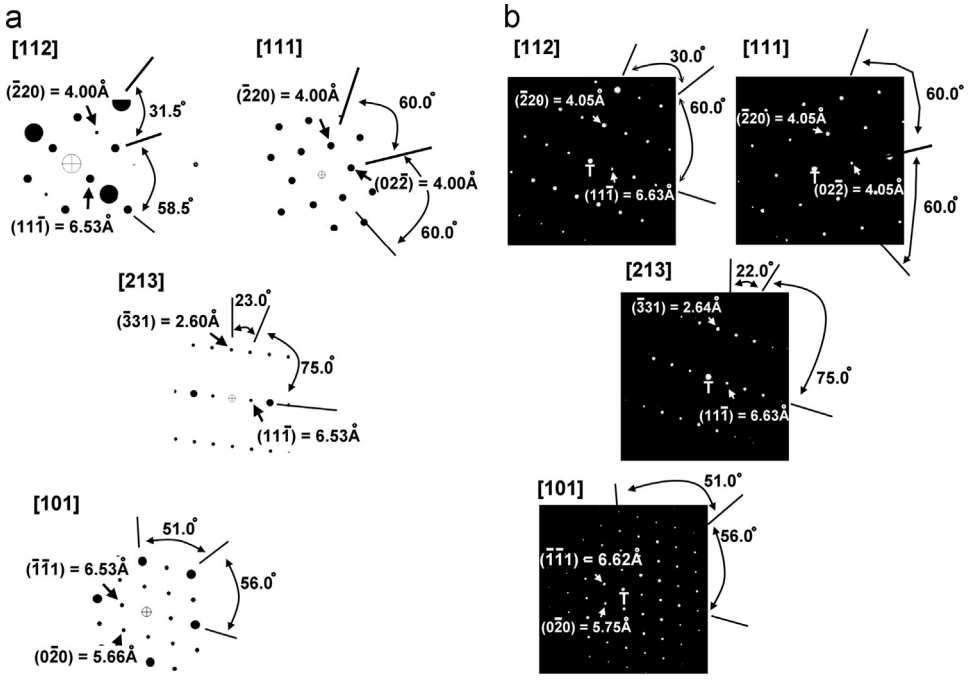


Fig. 5. (a and b) the simulated and experimental selected area diffraction patterns (SADPs) of $Fe_2Ti_4O$ with zone axes of [112], [111], [213], and [101], respectively.

### 3.3. Mechanical properties and hermeticity testing

Fig. 7(a and b) are schematic diagrams showing applied load, and supporting and bonded areas for the cross-bonded samples used in tensile and shear bond strength tests following the international standard ISO 13124:2011 (E) [28]. The steel and YSZ were prepared as rectangular bars (4 mm × 4 mm × 15 mm) and joined by Ag–26.7Cu–4.5Ti interlayer perpendicularly and symmetrically within $\pm 1^\circ$ as shown in Fig. 7(c). A cross-bonded sample was loaded in compression which yielded tensile or shear stress in the interface until the inception of debonding. The test was performed at a constant cross-head displacement rate of 0.5 mm/min. The load at fracture and the bonded area were used to compute the tensile and shear bond strength. The tensile and shear strengths of the steel/Ag–26.7Cu–4.5Ti interlayer/YSZ joint were measured as $16.7 \pm 4.8$ and $40.2 \pm 8.2$ MPa, respectively. Observations of the de-bonded samples revealed that fracture in all tested joints had occurred at the YSZ/interlayer interface and not at the steel/interlayer interface, indicating that the strength of the steel/interlayer interface was greater than that of the YSZ/interlayer interface. In earlier studies [8,14], the shear strength of YSZ/steel joints was reported to be 45∼100 MPa for the 316 stainless steel/63Ag–35.25Cu–1.75Ti interlayer/PSZ joint and 60∼90 MPa for 1Cr–18Ni–9Ti stainless steel/Ag–38Cu–5Ti interlayer/$ZrO_2$ joint, respectively. The shear strength in the present study for the YSZ/steel joint with an Ag–26.7Cu–4.5Ti interlayer was a little different than the previous results [8,14], probably due to the differences in the composition of Ag–Cu–Ti interlayer, the measurement techniques, and the joining conditions.

Fig. 8(a and b) displays schematic perspective and cross-sectional diagrams of the hermetic test samples in which a hole of 2.5 mm diameter was drilled in the center of the steel. Were pores and/or hairline cracks to exist at the steel/interlayer/YSZ interface, the helium gas would have penetrated such pores and cracks, resulting in an increase in the gas leak rates. The hermetic test sample of steel/Ag–26.7Cu–4.5Ti/YSZ joint is shown in Fig. 7(c). The leak rates for the isolated steel and YSZ bulk specimens had been measured separately and found to be $1.0 \times 10^{-9}$ and $3.8 \times 10^{-9}$ mbar $\ell$/s. In general, the acceptable leak rates for technical applications is in the range $10^{-6}$ to $10^{-8}$ mbar $\ell$/s but for vacuum tight components, the leak rates should be less than $10^{-8}$ mbar $\ell$/s. In the hermetic test of the steel/Ag–26.7Cu–4.5Ti interlayer/YSZ joints, the leak rate was measured as $1.5 \pm 1.1 \times 10^{-9}$ mbar $\ell$/s, indicating the joint had good hermeticity.

Fig. 9(a) shows the hardness ($H$) and elastic modulus ($E$) of the 27 indents across the steel/Ag–26.7Cu–4.5Ti interlayer/YSZ joint. Following nano-indentation testing, SEM and optical microscope (OM) images were used to identify the locations of the indents within the stainless steel, Ag–26.7Cu–4.5Ti interlayer, YSZ, and reaction products, respectively. The $H$ and $E$ values are 3.0 GPa and 224.6 GPa (average of the indents 1–6) for the stainless steel, 1.3 GPa and 107.0 GPa (average of the indents 12–16) for Ag–26.7Cu–4.5Ti interlayer, and 16.8 GPa and 230.5 GPa (average of the indents 18–27) for the YSZ, respectively. It should be noted that the hardness at the indent 10 near the interface of the steel/Ag–26.7Cu–4.5Ti interlayer, corresponding to the $Fe_2Ti$ phase observed in SEM and TEM images (Figs. 1(b) and 3(a)), suddenly increased to 13.3 GPa compared with that of steel

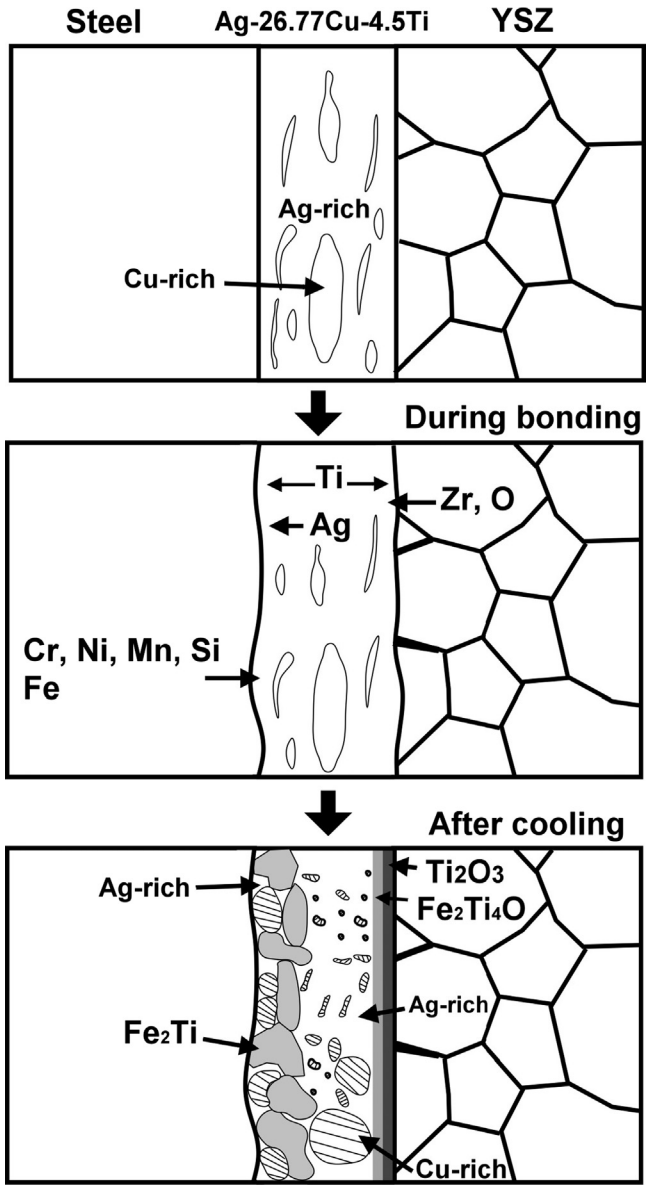


Fig. 6. Schematic diagram of the microstructural evolution of the steel/Ag–26.7Cu–4.5Ti/YSZ joint following one complete thermal cycle.

and interlayer. In contrast to the hardness at the YSZ/Ag–26.7Cu–4.5Ti interlayer interface, the *H*-value of the indent 17, corresponding with the $Fe_2Ti_4O$ and/or $Ti_2O_3$ region, was 19.0 GPa; this value is slightly higher than the *H*-value of the YSZ (~16.8 GPa). Fig. 9(b) shows the typical load versus depth curves of the 27 indents, displaying the plastic and elastic behaviors of the steel, Ag–26.7Cu–4.5Ti interlayer, YSZ, and the reaction products, respectively. Upon unloading, the Ag–26.7Cu–4.5Ti interlayer (indent 15) recovered 30 nm of the total 360 nm indentation depth, which corresponded to an elastic recovery of 8.3%. Moreover, the elastic recovery was 10.1% for the steel (indent 14), 39.4% for the $Fe_2Ti$ (indent 10), 53.3% for the YSZ (indent 18), and 53.1% for the $Fe_2Ti_4O$ and/or $Ti_2O_3$ regions (indent 17), respectively. Thus, the deformation behavior of YSZ, $Fe_2Ti$, and $Fe_2Ti_4O$ and/or $Ti_2O_3$ region was found to be both elastic and plastic, while the deformation behavior of the Ag–26.7Cu–4.5Ti interlayer and the steel was primarily plastic.

To sum up, the microstructure of the steel/Ag–26.7Cu–4.5Ti interlayer/YSZ joint and its physical and mechanical properties such as hermeticity, joint strength, and hardness were influenced by the type, spatial distribution and inherent mechanical behaviors of the reaction products that formed at YSZ/interlayer and steel/interlayer interfaces. At the steel/interlayer interface, hard and brittle $Fe_2Ti$ formed from the reaction of the Ti of the interlayer with Fe of the steel. The hardness of the $Fe_2Ti$ phase is high, about 13.3 GPa, greater than that of steel (3.0 GPa) and the interlayer (1.3 GPa). But, the load versus depth curves in Fig. 9(b) revealed that $Fe_2Ti$ had 60.6% plastic deformation (39.4% elastic recovery) that may have facilitated residual stress relief. Besides, $Fe_2Ti$ had particle-like morphology and it was distributed within the Ag-rich and Cu-rich phases to form a complex reaction layer. The Ag-rich and Cu-rich phases experienced very high plastic deformation, about 91.7% (low elastic recovery), that mitigated residual stress caused by the CTE mismatch between the steel and the interlayer. Thus, no cracks formed at the steel/interlayer interface as confirmed from the SEM and TEM images. In contrast to the YSZ/interlayer interface, the hardness of the $Fe_2Ti_4O$ and $Ti_2O_3$ reaction layers was high, close to 19.0 GPa, and they experienced only 46.9% plastic deformation (53.1% elastic recovery). Compared with the complex reaction layer composed of $Fe_2Ti$, Ag-rich, and Cu-rich phases at the steel/interlayer interface, the $Fe_2Ti_4O$ and $Ti_2O_3$ reaction layers at the YSZ/interlayer interface were harder and underwent less plastic deformation, probably resulting in the fracture at the YSZ/interlayer interface as confirmed by the observation of the de-bonded joints following strength testing. However, no cracks formed either at the YSZ/interlayer interface or at the steel/interlayer interface in as-fabricated joints and the leak rate was about $1.5 \pm 1.1 \times 10^{-9}$ mbar $\ell$/s, indicating the joints had good hermeticity.

## 4. Conclusions

1. A commercial Ag–26.7Cu–4.5Ti (in wt%) interlayer was used to join YSZ to a corrosion-resistant ferritic stainless steel for SOFC applications. The SEM and TEM coupled with EDS were used to characterize the microstructures of the interlayer, matrix, and the interlayer/steel and interlayer/YSZ interfaces.
2. In the steel/Ag–26.7Cu–4.5Ti interlayer/YSZ joint, the Fe from the steel dissolved into the interlayer to react with Ti to form a $Fe_2Ti$ phase, which also had Ag-rich and Cu-rich phases combined in a complex reaction layer at the steel/Ag–26.7Cu–4.5Ti interface.
3. At the Ag–26.7Cu–4.5Ti interlayer/YSZ interface, Ti from the interlayer reacted with the oxygen of YSZ to form a reaction layer of $Ti_2O_3$ at the interface and the Fe from the steel diffused across the interface layer toward YSZ to react with $Ti_2O_3$ to form a reaction layer of $Fe_2Ti_4O$.
4. The strength of the steel/metallic interlayer/YSZ joint was evaluated according to the newest method per “ISO

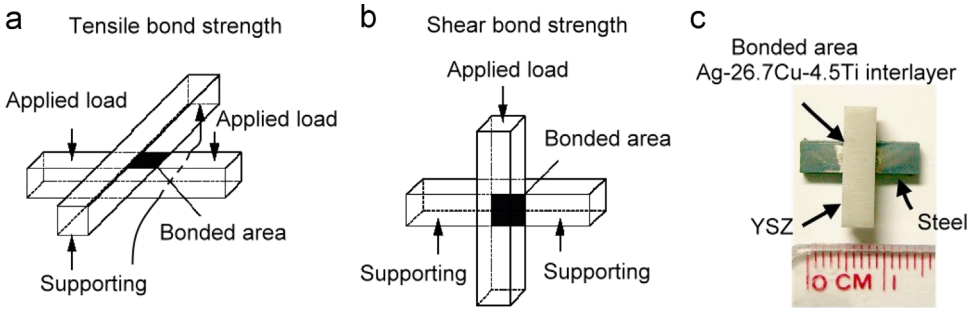


Fig. 7. (a, b) Schematic diagrams of applied load, support and bonded area for the cross-bonded samples in the tensile and shear bond strength tests per ISO-13124, and (c) photograph of the tensile and shear strength test sample of steel/Ag–26.7Cu–4.5Ti/YSZ joint.

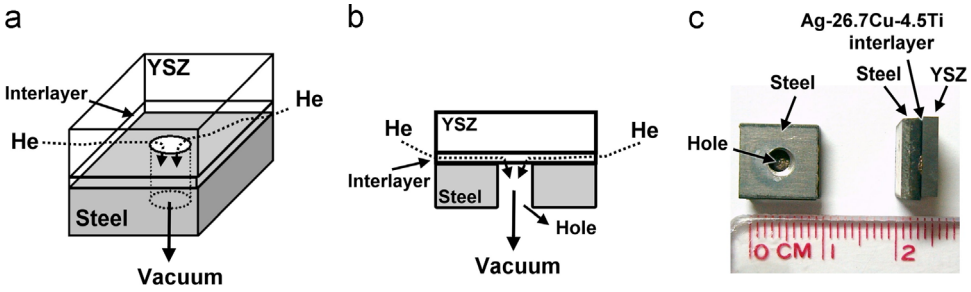


Fig. 8. (a, b) Schematic perspective and cross-sectional diagrams of the hermetic test sample, and (c) photograph of the hermetic test samples of steel/Ag–26.7Cu–4.5Ti/YSZ joint.

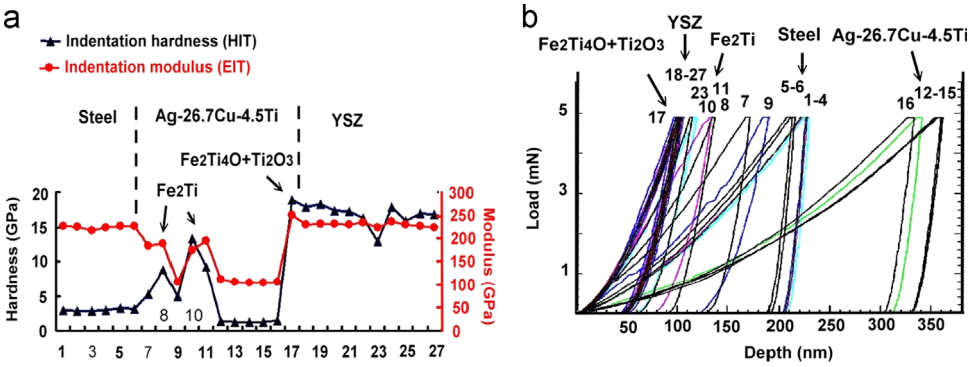


Fig. 9. (a) Hardness and elastic modulus of 27 indents across the steel/Ag–26.7Cu-4.5Ti/YSZ joint, and (b) typical load versus depth curves of 27 indents.

13124". The tensile and shear strengths of the steel/Ag–26.7Cu–4.5Ti interlayer/YSZ joint were $16.7 \pm 4.8$ and $40.2 \pm 8.2$ MPa, respectively. The leak rate of steel/Ag–26.7Cu–4.5Ti interlayer/YSZ joint was measured as $1.5 \pm 1.1 \times 10^{-9}$ mbar $\ell$/s, indicating the joints had good hermeticity.

5. The hardness ($H$) and elastic modulus ($E$) across the joints were characterized with a nanoindenter. The hardness of the $Fe_2Ti$ phase at the interface of steel/Ag–26.7Cu–4.5Ti interlayer abruptly increased to 13.3 GPa compared with that of steel (3.0 GPa) and Ag–26.7Cu–4.5Ti interlayer (1.3 GPa). The hardness of the $Fe_2Ti_4O$ and/or $Ti_2O_3$ region at the YSZ/Ag–26.7Cu–4.5Ti interlayer interface was measured as 19.0 GPa that was a little higher than the hardness of YSZ (~16.8 GPa). During strength testing, fracture in all samples occurred at the YSZ/Ag–26.7Cu–4.5Ti interlayer interface possibly because the $Fe_2Ti_4O$ and $Ti_2O_3$ layers had low plasticity relative to the complex reaction layer at the steel/interlayer (Table 1).

Table 1
Tensile and shear strengths, and hermeticity of steel/Ag–26.7Cu-4.5Ti/YSZ joint.

| Property | Value |
|---|---|
| Tensile strength (MPa) | $16.69 \pm 4.75$ |
| Shear strength (MPa) | $40.15 \pm 8.18$ |
| Leak rate (mbar $\ell$/s) | $1.53 \pm 1.05 \times 10^{-9}$ |

## Acknowledgments

The authors would like to thank the National Science Council of Taiwan for financially supporting this research under Contract No. NSC 101-2221-E-492-008.

## References

[1] P.A. Lessing, A review of sealing technologies applicable to solid oxide electrolysis cells, Journal of Materials Science 42 (2007) 3465–3476.
[2] K.S. Weil, C.A. Coyle, J.S. Hardy, J.Y. Kim, G.G. Xia, Alternative planar SOFC sealing concepts, Fuel Cells Bulletin 5 (2004) 11–16.
[3] J.W. Fergus, Materials challenges for solid-oxide fuel cells, JOM (2007) 56–59.
[4] B. Kuhn, E. Wessel, J. Malzbender, R.W. Steinbrech, L. Singheiser, Effect of isothermal aging on the mechanical performance of brazed ceramic/metal joints for planar SOFC-stacks, International Journal of Hydrogen Energy 35 (17) (2010) 9158–9165.
[5] J.W. Fergus, Sealants for solid oxide fuel cells, Journal of Power Sources 147 (1–2) (2005) 46–57.
[6] K.S. Weil, The state-of-the-art in sealing technology for solid oxide fuel cells, JOM 58 (8) (2006) 37–44.
[7] M. Singh, T.P. Shpargel, R. Asthana, Brazing of yttria-stabilized zirconia (YSZ) to stainless steel using Cu, Ag, and Ti-based brazes, Journal of Materials Science 43 (2008) 23–32.
[8] W.B. Hanson, K.I. Ironside, J.A. Fernie, Active metal brazing of zirconia, Acta Materialia 48 (2000) 4673–4676.
[9] H.Q. Hao, Y.L. Wang, Z.H. Jin, X.T. Wang, Joining of zirconia to zirconia using Ag–Cu–Ti filler metal, Journal of Materials Processing Technology 52 (1995) 238–247.
[10] H.Q. Hao, Y.L. Wang, Z.H. Jin, X.T. Wang, Joining of zirconia ceramic to stainless steel and to itself using $Ag_{57}Cu_{38}Ti_5$ filler metal, Journal of the American Ceramic Society 78 (81) (1995) 2157–2160.
[11] D. Sciti, A. Bellosi, L. Esposito, Bonding of zirconia to super alloy with the active brazing technique, Journal of the European Ceramic Society 21 (2001) 45–52.
[12] M.L. Muolo, E. Ferrera, L. Morbelli, Wetting, spreading and joining in the alumina–zirconia–inconel 738 system, Scripta Materialia 50 (2004) 325–330.
[13] W. Kobsiriphat, S. Barnett, Ag–Cu–Ti braze materials for sealing SOFCs, Journal of Fuel Cell Science and Technology 5 (011002-1) (2008) 7.
[14] J.S. Pimenta, A.J.A. Buschinelli, R.M. do Nascimento, A.E. Martinelli, J. Remmel, Joining of zirconia mechanically metallized with titanium, Cerâmica 56 (2010) 212–221.
[15] K.L. Lin, M. Singh, R. Asthana, Interfacial characterization of YSZ-to-steel joints with Ag–Cu–Pd interlayers for solid oxide fuel cell applications, Ceramics International 38 (2012) 1991–1998.
[16] A.V. Durov, B.D. Kostjuk, A.V. Shevchenko, Y.V. Naidich, Joining of zirconia to metal with Cu–Ga–Ti and Cu–Sn–Pb–Ti fillers, Materials Science and Engineering A 290 (2000) 186–189.
[17] A.V. Durov, Y.V. Naidich, B.D. Kostyuk, Investigation of interaction of metal melts and zirconia, Journal of Materials Science 40 (9–10) (2005) 2173–2178.
[18] M. Singh, T.P. Shpargel, R. Asthana, Braze oxidation behavior and joint microstructure in YSZ/steel joints using palladium brazes for SOFC applications, Materials Science and Engineering A 485 (2008) 695–702.
[19] M. Singh, T.P. Shpargel, R. Asthana, Brazing of stainless steel to yttria-stabilized zirconia using gold-based brazes for solid oxide fuel cell applications, International Journal of Applied Ceramic Technology 4 (2) (2007) 119–133.
[20] K.S. Weil, J.P. Rice, Substrate effects on the high-temperature oxidation behavior of a gold-based braze filler metal, Scripta Materialia 52 (2005) 1081–1085.
[21] K.L. Lin, M. Singh, R. Asthana, TEM characterization of Au-based alloys to join YSZ to steel for SOFC applications, Materials Characterization 63 (2012) 105–111.
[22] A. Tsoga, A. Naoumidis, P. Nikolopoulos, Wettability and interfacial reactions in the systems Ni/YSZ and Ni/Ti–$TiO_2$/YSZ, Acta Materialia 44 (9) (1996) 3679–3692.
[23] M.C. Tucker, C.P. Jacobson, L.C. De Jongh, S.J. Visco, A braze system for sealing metal–supported solid oxide fuel cells, Journal of Power Sources 160 (2) (2006) 1049–1057.
[24] R. Arroyave, Thermodynamics and kinetics of ceramic/metal interfacial interactions (Ph.D. dissertation), MIT, Cambridge, MA, USA, 2004.
[25] X.M. Xue, J.T. Wang, Z.T. Sui, Wettability and interfacial reactions of alumina and zirconia by reactive Ag–In base alloy at mid-temperatures, Journal of Materials Science 28 (1993) 1317–1322.
[26] V.M. Perevertailo, O.B. Loginova, N.G. Bagno, Interaction between metal melts and zirconium dioxide, Trans Joining and Welding Research Institute (Osaka) 30 (2001) 143–147.
[27] G. Cliff, G.W. Lorimer, The quantitative analysis of thin specimens, Journal of Microscopy 130 (3) (1975) 203–207.
[28] ISO 13124:2011, Fine ceramics (advanced ceramics, advanced technical ceramics) – Test method for interfacial bond strength of ceramic materials.
[29] W.C. Oliver, G.M. Pharr, An improved technique for determining hardness and elastic modulus using load and displacement sensing indentation experiments, Journal of Materials Research 7 (1992) 1564–1583.
[30] Z. Mei, Y.W. Yan, K. Cui, Effect of matrix composition on the microstructure of in situ synthesized TiC particulate reinforced iron-based composites, Materials Letters 57 (2003) 3175–3181.
[31] Z. Yu, P. Yang, K. Qi, R. Li, Effects of Mo interlayer on suppressing cracks in $Al_2O_3$/Kovar brazed joint, Rare Metal Materials and Engineering 37 (12) (2008) 2118–2121.
[32] K.L. Lin, M. Singh, and R. Asthana, Characterization of stainless steel/yttria-stabilized-zirconia interfaces with gold-based interlayers, 2013, unpublished research.
[33] W.C. Lee, O.Y. Kwon, and C.S. Kang, Microstructural characterization of interfacial reaction products between alumina and braze alloy, Journal of Materials Science., 30 (1995) 1679 – 1688.